Magnetic Resonance Imaging 57 (2019) 271–276

Contents lists available at ScienceDirect

Magnetic Resonance Imaging

journal homepage: www.elsevier.com/locate/mri

# Combination of free-breathing radial 3D fat-suppressed T1-weighted gradient-echo sequence with diffusion weighted images: Potential for differentiating malignant from benign peripheral solid pulmonary masses

Shan Dang[a,1], Xiang Gao[b,1], Guangming Ma[a], Nan Yu[a], Dong Han[a], Qi Yang[a], Xin Tian[a], Haifeng Duan[a,*]

[a] Department of Radiology, The affiliated hospital of Shaanxi university of Chinese medicine, Xian Yang, China
[b] Department of Clinical Lab, Nuclear Industry 215 Hospital of Shaanxi Province, Xian Yang, China

ARTICLE INFO

*Keywords:*
Free-breathing radial T1-weighted gradient echo sequence
Radial volumetric interpolated breath-hold (radial VIBE) sequence
Diffusion magnetic resonance imaging
Lung MRI
Multidetector computed tomography

ABSTRACT

*Objectives:* High resolution CT is the most commonly used radiological method for differentiating benign from malignant peripheral solid pulmonary masses, however, some of them are not easily diagnosed by morphology alone. Furthermore, due to the radiation dose, it is unsuitable for patients with disorders requiring repeated examinations over prolonged periods. The aims of this study were to evaluate whether a combination of diffusion-weighted images (DWI) and free-breathing radial 3D fat-suppressed T1-weighted gradient echo (radial volumetric interpolated breath-hold examination, radial VIBE) sequence can enable discrimination between benign from malignant peripheral solid pulmonary masses.

*Materials and methods:* Both chest CT scan and MR imaging with radial VIBE and DWI were obtained from 47 patients; 30 males and 17 females (mean age 64 years old; age range 48–83 years old). Benign and malignant peripheral solid pulmonary masses were conclusively identified by pathology results. Two radiologists independently reviewed all the images and record radiological features including morphological signs on radial VIBE, CT images, and ADC value. Receiver operating characteristic (ROC) was used to analyze the capability of radial VIBE as well as DWI to distinguish malignant from benign peripheral solid pulmonary masses.

*Results:* In 77% of patients, malignant peripheral solid pulmonary masses were found. Morphological signs of mediastinal lymph node enlargement and lobulation were more easily found in malignant masses in both radial VIBE (mediastinal lymph node enlargement: $p = 0.033$, lobulation: $p = 0.039$) and CT (mediastinal lymph node enlargement: $p = 0.004$, lobulation: $p = 0.012$). The ADC value were also significant difference between benign and malignant groups ($p = 0.001$). Combined ADC value with radial VIBE was a most specific test than routine-dose CT (86.1% vs 75%, $p < 0.001$), but less sensitive than routine-dose CT (81.8% vs 90.9%; $p < 0.001$) for malignant peripheral solid pulmonary masses detection. Diagnostic accuracy was 89% for combining ADC value with radial VIBE, and 85% for routine-dose CT.

*Conclusions:* Combination of morphological signs and ADC value seems to improve differentiating malignant from benign peripheral solid pulmonary masses. Especially in patients unable to endure radiation exposure, suspend respiration, radial VIBE provides similar morphological signs displaying to those on routine-dose CT.

## 1. Introduction

Lung cancer has become the most common cancer worldwide and is also the most common cause of cancer-related deaths, with a high incidence in East Asia [1]. Differentiation between benign and malignant pulmonary solitary lesions is often difficult [2] due to limited radiological information. Observing the morphological features of peripheral solid pulmonary masses can help to distinguish between those that are malignant and benign [3]. High resolution CT is the most commonly used radiological method for differentiating benign from malignant peripheral solid pulmonary masses [4], however, some of them are not easily diagnosed by morphology alone. Furthermore, due

* Corresponding author at: Department of Radiology, The affiliated hospital of Chinese traditional medical university, 2# Weiyang Western Road, Xian Yang 712000, China.
*E-mail address:* 896465691@qq.com (H. Duan).
[1] Shan Dang and Xiang Gao contributed equally to this work.

https://doi.org/10.1016/j.mri.2018.12.004
Received 26 June 2018; Accepted 8 December 2018

to the radiation dose, it is unsuitable for patients with disorders requiring repeated examinations over prolonged periods [5]. A recent large high-quality RCT (the NLST) found that annual low-dose CT screening reduced the relative risk of death from lung cancer by 20% [6], but the absolute risk by 0.33% in a population with a substantially elevated risk for lung cancer [7].

Magnetic resonance imaging (MRI) can provide morphological and functional information with multiple sequences and high resolution of soft tissue, as well as avoiding radiation exposure. Chest MRI has faced great challenges due to the lack of H protons and low signal-to-noise ratio in normal lung tissue. However, over recent years, MRI has made great progress in terms of hardware and software, with the image quality becoming better and better [8]. In particular, for patients who cannot hold their breath, respiratory gating or diaphragm navigation can also be used, nevertheless, the acquisition time of enhanced scanning is prolonged [9]. The free-breathing radial 3D fat-suppressed T1-weighted gradient echo sequence (radial-VIBE) (section thickness: 1.2 mm) using radial k-space data sampling has been demonstrated to substantially reduce motion-related artifacts, and can compensate for breathing, heart and large blood vessel pulsation and other motion artifacts, providing high-resolution imaging [10]. Recently published studies have demonstrated that radial VIBE can improve image quality for adult and pediatric abdominopelvic, esophageal cancer and head and neck imaging [9,11–14]. In addition, a study by Ohno Y et al. reported the capability of nodule detection, nodule type assessment and pulmonary parenchyma disease assessment using high-resolution MR ultrashort TE (compared with thin-section standard-and low-dose computed tomography) [15,16]. However, reports of the usefulness of MRI in observing the morphological characteristics of peripheral solid pulmonary masses are rare, especially using radial VIBE. Moreover, DWI has been widely used in most organs of the body, with published studies showing that DWI may be a useful tool for distinguishing malignant from benign pulmonary lesions by measuring the ADC value [17,18].

We hypothesized that pulmonary thin-section radial VIBE combined with the ADC value may improve the diagnostic confidence of peripheral solid pulmonary masses due to morphological and functional information. Thus, the purpose of the present study was to evaluate the diagnostic capability of no radiation-dose MRI (the ADC value combined with radial VIBE) in differentiating malignant from benign peripheral solid pulmonary masses.

## 2. Materials and methods

### 2.1. Subjects

The present study was approved by the institutional review board, and written informed consent was obtained from each patient. A prospectively populated research database was searched for patients who underwent routine-dose CT and state-of-the-art MRI of the lung with radial VIBE and DWI from 10/2016 to 01/2018 and fulfilled the following inclusion criteria: suspected peripheral lung cancer who underwent both chest routine-dose thin-section CT and MRI (radial VIBE and DWI), the CT image quality was sufficient for diagnosis, and MR examination was performed within 48 h after CT examination. Exclusion criteria were: (1) contraindication to MR (pacemaker, ferromagnetic implants, claustrophobia, etc.) (2) poor MR image quality. Seven patients were excluded due to poor MR image quality (finally determined by consensus of two radiologists). Following exclusions, the present study group was comprised of 47 patients, with 30 males and 17 females (mean age 64 years old; age range 48–83 years old), 47 lung masses, 36 malignant masses (20 adenocarcinoma, 5 squamous cell carcinoma, 6 small cell carcinoma, 1 giant cell carcinoma, 1 carcinoid tumor, 1 metastasis, 1 adenosquamous), 11 benign masses (3 chronic inflammation, 1 tuberculoma, 2 organizing pneumonia, 1 inflammatory pseudotumor, 1 pulmonary abscess, 1 pulmonary sequestration, 1 pneumonia, and 1 other). Benign and malignant masses were conclusively identified from pathology results. Most of the masses were treated using transthoracic needle biopsy, however, a few patients were completely surgically resected.

### 2.2. CT protocol

All chest routine-dose thin-section CT examinations were performed with a 64-detector row CT scanner (Discovery CT750 HD, GE Healthcare, USA). The scanning range was from the thoracic entrance to 2 cm below the diaphragm, using the following parameters; tube voltage: 80/140 KV instantaneous switching, tube current: 260 mA, rotation time: 0.5 s/rot, matrix: 512 × 512. All routine-dose thin-section CT images of 1.2 mm section thickness were reconstructed for the lung window setting and the mediastinal window setting. The CT images were displayed in standard lung (W 1200 HU, C −600 HU) and mediastinal (W 350 HU, C 40 HU) window settings.

### 2.3. High-resolution pulmonary MR imaging with radial VIBE and DWI

MR imaging was performed with a 3 Tesla MR-Scanner (MAGNETOM Skyra, Siemens Healthcare, Erlangen, Germany) using an 18-element body surface coil. The routine MRI protocol covers the chest, with sequences including axial radial VIBE, axial DWI with b value of 0 and 800 s/mm$^2$. In each patient, pulmonary thin-section radial VIBE was performed with a free-breathing radial 3D fat-suppressed T1-weighted gradient echo sequence (repetition time: [TR] 2.79 ms, echo time [TE] 1.39 ms; voxel size: 1.2 × 1.2 × 1.2 mm$^3$; flip angle: 5°; reconstruction matrix: 320 × 320, field of view: 380 mm; scan time: 5 min 30 s). DWI (b = 0,800 s/mm$^2$): TR: 7100 ms, TE: 58 ms, voxel size: 1.6 × 1.6 × 5.0 mm, flip angle: 5°; NEX: 1 (b = 0 s/mm$^2$), 4(b = 800 s/mm$^2$), matrix: 400 × 320, FOV 400 mm, scan time: 2 min 43 s.

### 2.4. Image analysis

The image quality of radial VIBE was evaluated by a chest radiologist with > 20 years' experience and a radiologist with 6 years of experience. A 5-point visual scoring system was used to evaluate radial VIBE image quality on chest imaging including: adopted; 1, non-diagnostic; 2, poor; 3, acceptable; 4, good; 5, excellent. The radial VIBE image quality of all the patients was evaluated by the two radiologists independently in different rooms. Patients with a score of < 3 points were excluded by consensus of the two observers.

The same two radiologists were blinded to clinical and histological findings. They reviewed both CT and radial VIBE imaging and record each masses and their morphological features, including lobulation, spiculation, calcification, halo, cavitation, bubble-like attenuation, convergence of vessels, pleural indentation and mediastinal lymph node enlargement. The order of observation is as follows. Firstly, the radial VIBE images of all the patients were evaluated by the two radiologists independently in different rooms. Secondly, radial VIBE images were reviewed repeatedly 2 weeks after first reading. Thirdly, the routine-dose CT images were observed by these two radiologists 2 weeks after radial VIBE images reading. Finally, routine-dose CT images were reviewed repeatedly 2 weeks after first reading. Both readers observed routine-dose thin-section CT images in lung (W 1200 HU, C −600 HU) and mediastinal (W 350 HU, C 40 HU) window settings. A 5-point visual scoring system (1, absent; 2, probably absent; 3, equivocal; 4, probably present; 5, present) was used to determine the presence of morphological characteristics of each mass in radial VIBE imaging. The display of morphological characteristics on CT images was divided into either “visible” or “invisible”.

For ADC value measurement, a round or elliptical region of interest (ROI) was placed on the solid area of the masses on ADC map. Areas of focal necrosis, large vessels and prominent artifacts were carefully avoided. A large as possible ROI was placed in the center of the lesion.

All measurements were performed three times at different image levels by the two radiologists independently, and average ADC values were calculated.

### 2.5. Statistical analysis

Statistical analyses were performed with the SPSS version 24.0 software (SPSS, Chicago, USA), and $p < 0.05$ was considered statistically significant. A weighted kappa test was carried out to determine intraobserver, interobserver and intermethod agreement based on consensus assessment for the capability to display morphological characteristics of peripheral solid pulmonary masses. Intraobserver, interobserver and intermethod agreement were considered as poor for $k < 0.21$, fair for $k = 0.21–0.40$, moderate for $k = 0.41–0.60$, substantial for $k = 0.61–0.80$, and excellent for $k = 0.81–1.00$ [21]. The chi-squared test was used to analyze the obtained values in the differential diagnosis of morphological characteristics. Before chi-squared test, the "1", "2" and "3" points of morphological characteristics in radial VIBE were defined as "invisible", "4" and "5" points were defined as "visible".

The ADC value conformed to normal distribution ($p = 0.195$), therefore, the data were subjected to a two-sample *t*-test. Multiple logistic regression analyses were performed to determine whether spiculation, lobulation, pleural indentation, bubble-like attenuation, calcification, cavitation, enlarged mediastinal lymph node, or presence of a halo were independently associated with a benign or malignant diagnosis. Receiver operating characteristic (ROC) analysis was used to evaluate the diagnostic capability of ADC and morphological characteristics with routine-dose CT and radial VIBE in the differentiation between malignant and benign peripheral solid pulmonary masses.

## 3. Results

A total of 47 peripheral solid pulmonary masses were observed, 36 malignant masses, 11 benign masses, the range of size was 1.1–8.2 cm, with an average diameter of 3.94 ± 1.91 cm.

### 3.1. Evaluation of image quality

All interobserver agreement for radial VIBE image quality were significant and excellent ($k = 0.89$, $p < 0.001$).

### 3.2. Evaluation of the capability to distinguish malignant from benign peripheral solid pulmonary masses

Intraobserver and interobserver agreement of morphological characteristics was significant and excellent in radial VIBE and routine-dose CT images ($k = 0.87–1.0$, $p < 0.001$).

Evaluation of morphological characteristics using routine-dose CT and radial VIBE of histologically-verified malignant and benign peripheral solid pulmonary masses (consensus readings) is shown in Table 1. No significant differences were found in the display of morphological characteristics with respect to internal characteristics, peripheral structure and visceral pleural indentation between benign and malignant peripheral solid pulmonary masses in images either obtained by radial VIBE or routine-dose CT. However, the morphological characteristics of mediastinal lymph node enlargement and lobulation shown in both radial VIBE (mediastinal lymph node enlargement: $p = 0.033$, lobulation: $p = 0.039$) and CT (mediastinal lymph node enlargement: $p = 0.004$, lobulation: $p = 0.012$) were more easily found in malignant peripheral solid pulmonary masses.

The representative images of routine-dose CT, radial VIBE, DWI and ADC maps are shown in Figs. 1–3. There was a significant difference in the ADC value between benign and malignant groups ($p = 0.001$), with a cut-off ADC value of $1197 \times 10^{-6}\,mm^2/s$.

### 3.3. Diagnostic capability of radial VIBE and ADC value

The diagnostic capabilities of the combination of radial VIBE and the ADC value, CT alone, radial VIBE alone, and the ADC value alone for distinguishing between benign and malignant peripheral solid pulmonary masses are shown in Table 2. According to the ROC curve, the area under the curve (AUC), sensitivity and specificity were 0.806, 81.8%, and 75%, respectively, for radial VIBE alone; and 0.851, 90.9%, and 75%, respectively, for routine-dose CT alone. The combination of radial VIBE and the ADC value obtained higher specificity (86.1%) and AUC (0.894) than CT or radial VIBE alone, but the less sensitive than only CT (81.8% vs 90.9%). The combination of radial VIBE morphological characteristics and the ADC value was able to distinguish between malignant and benign peripheral solid pulmonary masses better than CT, ADC value, or radial VIBE alone.

## 4. Discussion

The present study shows that in comparison with CT, imaging with radial VIBE was useful in displaying the morphological characteristics of peripheral solid pulmonary masses. Intraobserver and interobserver agreement was significant and excellent. Among these morphological characteristics, only mediastinal lymph node enlargement and lobulation could be used to distinguish malignant from benign peripheral solid pulmonary masses in routine-dose CT and radial VIBE images. The diagnostic capability of only radial VIBE was slightly lower than CT in distinguishing malignant from benign peripheral solid pulmonary masses. However, the diagnosis capability was better by combining radial VIBE with the ADC value than only CT.

A previous study focused on the morphological characteristics of SPN with an ECG gated gradient echo sequence, showing that the diagnostic performance of MRI was found to be comparable to conventional helical CT in differentiating malignant from benign solitary pulmonary nodules [22]. Traditional MRI sequences cannot adequately display the morphological signs of pulmonary lesions due to large section thickness and obvious motion-related artifacts, however, the recently developed free-breathing radial-VIBE sequence uses radial k-space data acquisition scheme, with the distinct advantage of a significantly lower sensitivity to motion [10]. Published studies have demonstrated that radial k-space sampling schemes can improve image quality in adult and pediatric abdominopelvic, esophageal cancer, head and neck imaging [9–14]. A study by Zhang, Qu et al., showed that contrast-enhanced radial VIBE is promising for esophageal cancer staging, not only for esophageal cancer in the mucosa but also invasion of the muscularis propria [14]. Chandarana, Kai et al. found improved image quality and higher lesion conspicuity with free-breathing radial gradient echo acquisition in pediatric patients undergoing contrast-enhanced abdominopelvic MRI than conventional T1-weighted examination (many pediatric patients cannot adequately suspend respiration, decreasing the image quality of the conventional contrast-enhanced T1-weighted examination), albeit at the cost of longer but clinically-acceptable acquisition times [9]. In the present study, the majority of morphological characteristics were evaluated in radial VIBE with "excellent" or "substantial" intermethod agreement with CT. Limitations of radial VIBE were found in identifying certain morphological characteristics including calcification, pleural indentation, halo, and short fine spiculation.

Additionally, the observation of lobulation has been used to distinguish between benign and malignant peripheral solid pulmonary masses with routine-dose CT [19] in literature, and had a differential capacity with radial VIBE or CT alone in this study. Furthermore, consistent with the literature, the presence of mediastinal lymph node enlargement in routine-dose CT images was also observed more frequently in malignant peripheral solid pulmonary masses [20], the display capability of radial VIBE images was as well as CT. However, the differences in spiculation, pleural indentation, convergence of vessels,

**Table 1**
Results of morphological characteristics evaluation using CT and radial VIBE of histologically-verified malignant and benign peripheral solid pulmonary masses (consensus readings).

| | | CT | | | Radial VIBE | | |
|---|---|---|---|---|---|---|---|
| | | Benign (11) | Malignant (36) | p | Benign (11) | Malignant (36) | p |
| Shape | Round/oval | 0 | 0 | n.s. | 0 | 0 | n.s. |
| | Smooth | 1 | 0 | n.s. | 1 | 0 | n.s. |
| | Lobulation | 1 | 21 | 0.012 | 1 | 18 | 0.039 |
| Peripheral structure | Spiculation | 5 | 25 | n.s. | 2 | 22 | n.s. |
| | Halo | 1 | 3 | n.s. | 0 | 1 | n.s. |
| Internal structure | Cavitation | 1 | 4 | n.s. | 1 | 4 | n.s. |
| | Calcification | 1 | 2 | n.s. | 0 | 2 | n.s. |
| | Bubble-like attenuation | 3 | 8 | n.s. | 2 | 4 | n.s. |
| | Convergence of vessels | 6 | 15 | n.s. | 3 | 12 | n.s. |
| Visceral pleural | Pleural indentation | 4 | 20 | n.s. | 2 | 14 | n.s. |
| Lymph node | Mediastinal lymph node enlargement | 0 | 17 | 0.004 | 1 | 17 | 0.033 |

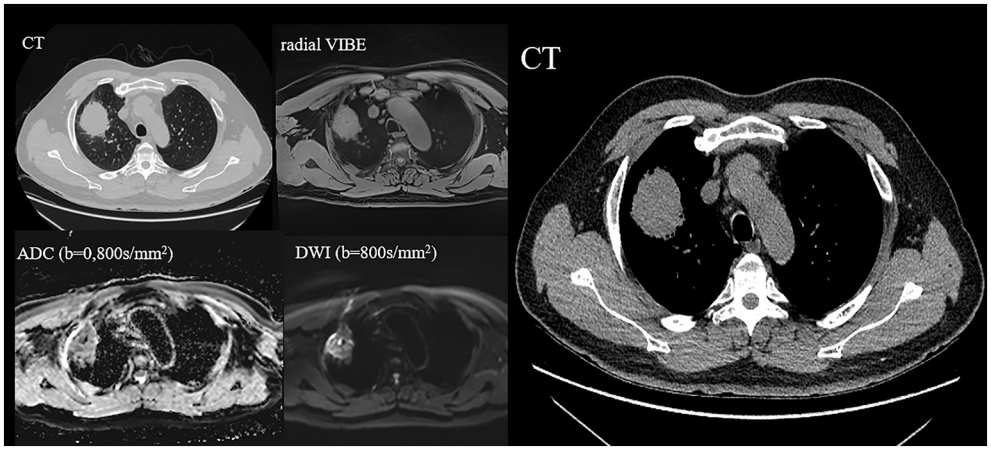


**Fig. 1.** 58-Year-old male, CT image shows solid pulmonary mass in right lung upper lobe (lung window), with homogeneous density (mediastinal window), the size of lesion was 6.1 cm × 4.7 cm. Radial VIBE image shows a small spot with low signal intensity in the center of the mass; the spot had high signal intensity in DWI (b = 800 s/mm$^2$), and low signal intensity in ADC map (b = 0, 800 s/mm$^2$). And the ADC value of the mass around the spot was 1690 × 10$^{-6}$ mm$^2$/s. The pathologic diagnosis was confirmed as inflammatory pseudotumor.

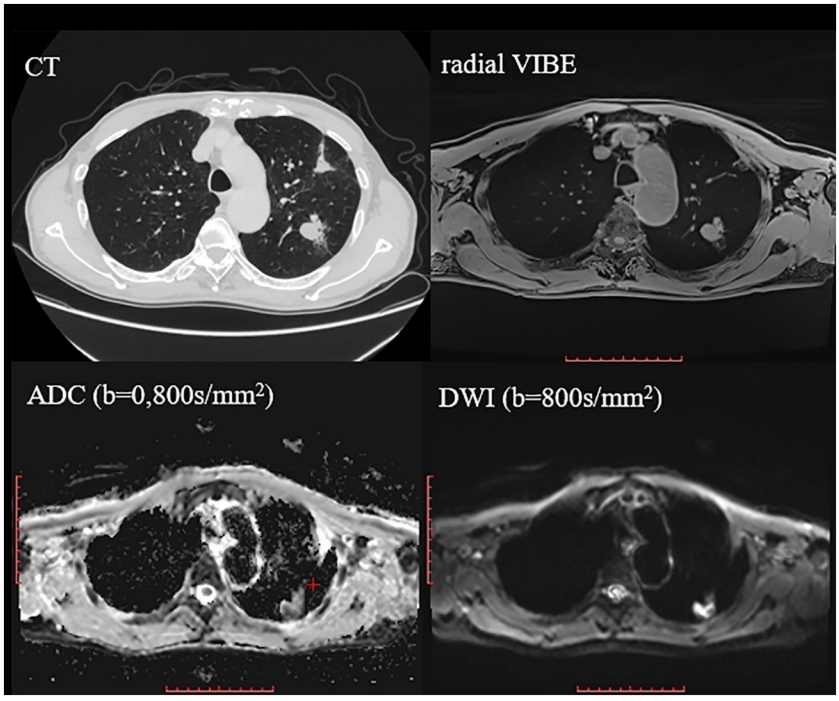


**Fig. 2.** Male, 73-year-old, the size of the lesion was 2.3 × 1.9 cm, bubble-like attenuation was visible inside the lesion in axial CT and radial VIBE. The irregular lesion shows high signal intensity in DWI (b = 800 s/mm$^2$), and low signal intensity in ADC map (b = 0, 800 s/mm$^2$), the ADC value of the lesion was 559.7 × 10$^{-6}$ mm$^2$/s. The pathologic diagnosis was confirmed as small-cell carcinoma.

and the presence of a halo, which also had value in differential diagnosis [2,19], were not observed between benign and malignant peripheral solid pulmonary masses in the present study, maybe due to the small size of sample.

Moreover, previous studies have shown that the ADC value is feasible in differentiating lung cancer from post-obstructive lobar collapse and may also be a useful tool for distinguishing malignant from benign pulmonary lesions and for differentiating small cell lung carcinoma and

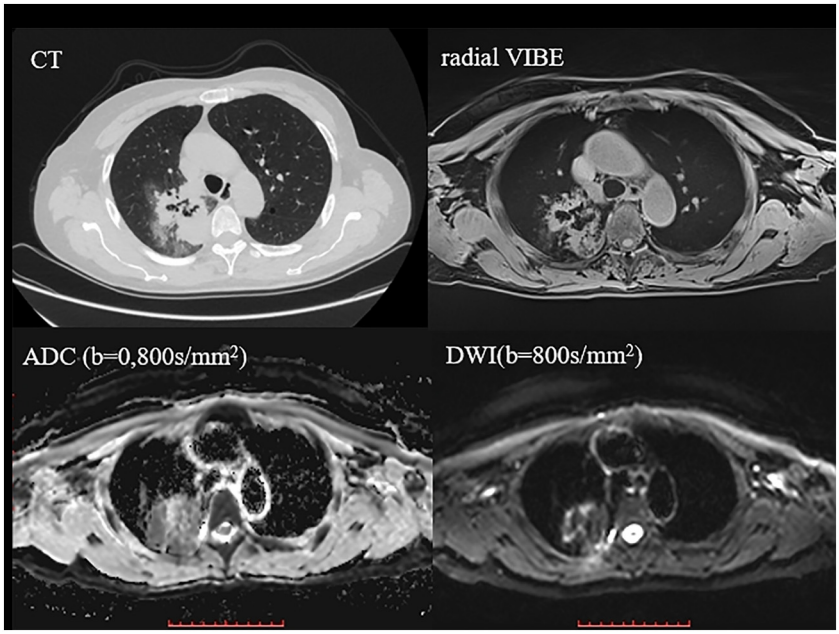


**Fig. 3.** A 64-year-old female; halo and cavitation were visible inside the lesion in axial CT and radial VIBE. The solid lesion shows high signal intensity in DWI (b = 800 s/mm$^2$), and low signal intensity in ADC map (b = 0, 800 s/mm$^2$), the ADC value of the lesion was 799 × 10$^{-6}$ mm$^2$/s, The pathologic diagnosis was confirmed as acinar adenocarcinoma.

**Table 2**
ROC analyses of diagnostic accuracy of radial VIBE + ADC value and only CT, radial VIBE, ADC value for distinguishing benign and malignant peripheral solid pulmonary masses.

| | Sensitivity (%) | Specificity (%) | AUC |
|---|---|---|---|
| Routine-dose CT | 90.9 | 75.0 | 0.85 |
| Radial VIBE | 81.8 | 75.0 | 0.80 |
| ADC value | 81.8 | 66.7 | 0.82 |
| ADC value and radial VIBE | 81.8 | 86.1 | 0.89 |

non-small cell lung cancer, and various subtypes of lung adenocarcinoma [17,18,23,24]. Consistent with this literature, the present study demonstrates that the ADC value can distinguish malignant from benign peripheral solid pulmonary masses. Nevertheless, combining radial VIBE with the ADC value will improve the capability of distinguishing malignant from benign peripheral solid pulmonary masses.

There are several limitations in the present study. Firstly, the small lung nodules (5–10 mm) and ground-glass nodules had not enrolled in this study. Secondly, when reviewing images, we could not guarantee that the CT and radial VIBE imaging were at the same level. Thirdly, radial VIBE requires higher respiratory rhythm for patients. The motion artifact of the lower lung near the diaphragm, heart, and large vessels is obvious when the breathing rhythm of patients is not stable, and further improved investigation is warranted.

In conclusion, although not as efficient as routine-dose CT, radial VIBE is a promising technique for observing the morphological characteristics of peripheral solid pulmonary masses. In addition, compared with routine-dose CT, combination radial VIBE with the ADC value can improve the diagnosis capability for distinguishing malignant from benign peripheral solid pulmonary masses for avoiding radiation exposure.

## References

[1] Ferlay J, Shin HR, Bray F, et al. Estimates of worldwide burden of cancer in 2008: GLOBOCAN 2008[J]. Int J Cancer 2010;127(12):2893–917.
[2] Seemann MD, Staebler A, Beinert T, et al. Usefulness of morphological characteristics for the differentiation of benign from malignant solitary pulmonary lesions using HRCT[J]. Eur Radiol 1999;9(3):409.
[3] Erasmus JJ, Connolly JE, Mcadams HP, et al. Solitary pulmonary nodules: part I. morphologic evaluation for differentiation of benign and malignant lesions[J]. Radiographics 2000;20(1):43–58.
[4] Brandman S, Ko JP. Pulmonary nodule detection, characterization, and management with multidetector computed tomography[J]. J Thorac Imaging 2011;26(2):90–105.
[5] Biederer J, Beer M, Hirsch W, et al. MRI of the lung (2/3). Why … when … how?[J]. Insights Imaging 2012;3(4):355–71.
[6] Heleno B, Rasmussen JF, Brodersen J. Reduced lung-cancer mortality with CT screening[J]. N Engl J Med 2011;365(21):2037–8.
[7] Bach PB, Mirkin JN, Oliver TK, et al. Benefits and harms of CT screening for lung cancer: a systematic review[J]. JAMA 2012;307(22):2418–29.
[8] Rajaram S, Swift AJ, Capener D, et al. Lung morphology assessment with balanced steady-state free precession MR imaging compared with CT[J]. Radiology 2012;263(2):569.
[9] Chandarana H, Kai TB, Winfeld MJ, et al. Free-breathing contrast-enhanced T1-weighted gradient-echo imaging with radial k-space sampling for paediatric abdominopelvic MRI[J]. Eur Radiol 2014;24(2):320.
[10] Chandarana H, Block TK, Rosenkrantz AB, et al. Free-breathing radial 3D fat-suppressed T1-weighted gradient echo sequence: a viable alternative for contrast-enhanced liver imaging in patients unable to suspend respiration[J]. Invest Radiol 2011;46(10):648–53.
[11] Wu X, Raz E, Block TK, et al. Contrast-enhanced radial 3D fat-suppressed T1-weighted gradient-recalled echo sequence versus conventional fat-suppressed contrast-enhanced T1-weighted studies of the head and neck[J]. AJR Am J Roentgenol 2014;203(4):883–9.
[12] Fujinaga Y, Ohya A, Tokoro H, et al. Radial volumetric imaging breath-hold examination (VIBE) with k-space weighted image contrast (KWIC) for dynamic gadoxetic acid (Gd-EOB-DTPA)-enhanced MRI of the liver: advantages over Cartesian VIBE in the arterial phase[J]. Eur Radiol 2014;24(6):1290–9.
[13] Azevedo RM, de Campos RO, Ramalho M, et al. Free-breathing 3D T1-weighted gradient-echo sequence with radial data sampling in abdominal MRI: preliminary observations[J]. AJR Am J Roentgenol 2011;197(3):650–7.
[14] Zhang F, Qu J, Zhang H, et al. Preoperative T staging of potentially resectable esophageal cancer: a comparison between free-breathing radial VIBE and breath-hold Cartesian VIBE, with histopathological correlation[J]. Transl Oncol 2017;10(3):324.
[15] Ohno Y, Koyama H, Yoshikawa T, et al. Pulmonary high-resolution ultrashort TE MR imaging: comparison with thin-section standard- and low-dose computed tomography for the assessment of pulmonary parenchyma diseases[J]. J Magn Reson Imaging 2016;43(2):512–32.
[16] Ohno Y, Koyama H, Yoshikawa T, et al. Standard-, reduced-, and no-dose thin-section radiologic examinations: comparison of capability for nodule detection and nodule type assessment in patients suspected of having pulmonary nodules[J]. Radiology 2017;284(2):562.
[17] Liu H, Liu Y, Yu T, et al. Usefulness of diffusion-weighted MR imaging in the evaluation of pulmonary lesions[J]. Eur Radiol 2010;20(4):807.
[18] Matoba M, Tonami H, Kondou T, Yokota H, Higashi K, Toga H, et al. Lung carcinoma: diffusion-weighted MR imaging–preliminary evaluation with apparent diffusion coefficient[J]. Radiology 2007;243(2):570–7.
[19] Zwirewich CV, Vedal S, Miller RR, et al. Solitary pulmonary nodule: high-resolution CT and radiologic-pathologic correlation[J]. Radiology 1991;179(2):469–76.
[20] Fukui T, Katayama T, Ito S, et al. Clinicopathological features of small-sized non-small cell lung cancer with mediastinal lymph node metastasis[J]. Lung Cancer 2009;66(3):309–13.
[21] Svanholm H, Starklint H, Gundersen HJ, et al. Reproducibility of histomorphologic diagnoses with special reference to the kappa statistic[J]. APMIS

1989;97(7–12):689–98.
[22] Schaefer JF, Vollmar J, Wiskirchen J, et al. Differentiation between malignant and benign solitary pulmonary nodules with proton density weighted and ECG-gated magnetic resonance imaging[J]. Eur J Med Res 2006;11(12):527–33.
[23] Qi LP, Zhang XP, Tang L, et al. Using diffusion-weighted MR imaging for tumor detection in the collapsed lung: a preliminary study[J]. Eur Radiol 2009;19(2):333–41.
[24] Tanaka R, Horikoshi H, Nakazato Y, et al. Magnetic resonance imaging in peripheral lung adenocarcinoma: correlation with histopathologic features[J]. J Thorac Imaging 2009;24(1):4–9.